17th World Conference on Earthquake Engineering, 17WCEE
Sendai, Japan - September 13th to 18th 2020

Estimation of strong motion generation area (SMGA) during the 2018 Hokkaido eastern Iburi earthquake

S. Kurahashi[(1)] and K. Irikura[(2)]

[(1)] *Associate Professor, Aichi Institute of Technology, susumu@aitech.ac.jp*
[(2)] *Visiting Professor, Aichi Institute of Technology, irikura@geor.or.jp*

Abstract

The strong motion generation area (SMGA) source model during the 2018 Hokkaido eastern Iburi earthquake (Mw6.6, depth: 37km) was estimated by the empirical Green's function method (EGFM) using strong motion data in 0.5-10Hz. First, a source fault model of the mainshock was assumed with three segments from distribution of aftershocks and observed waveforms with three wavepackets. A rupture starting point of each SMGA was determined from the onset of each wavepacket seen in the observed records assuming the source fault plane. Second, observed records of two aftershocks (EGF1 and EGF2 events) are used as the empirical Green's functions. EGF1 and EGF2 occurring nearby SMGA1 and SMGA2, respectively, are for SMGA1 and SMGA2. EGF2 is also used for SMGA3because SMGA2 and SMGA3 are close to each other. The stress parameter and area of each EGF event were estimated from corner frequency evauated by the source spectral ratios of the mainshock to the EGF events. Third, the synthetic motions from the mainshock are estimated for assumed SMGA model using the EGFM. The best-fit SMGA source model was obtained to minimize the residuals between the observed and synthetic waveforms. As a result, the best-fit SMGA source model consists of three SMGAs (SMGA1-3) located in the southern segment and the northern segment, respectively. The stress parameter of each SMGA is 27-35MPa and higher than those of shallow inland crustal earthquakes. The combined area of SMGAs area is 90.38km^2 and deviates smaller from the relationship between seismic moment and the combined area of asperities in the conventional scaling relation. Finally, we estimated the stress parameters of 17 aftershocks (Mw4.0-Mw4.9) occurring in and around the source area of the mainshock from their corner frequencies using the source spectral ratio method. The stress parameters of the aftershocks depend on source depth.

Keywords: the 2018 Hokkaido eastern Iburi earthquake, strong motions generation area (SMGA), stress parameter

1. Introduction

On 6 September 2018, an Mw 6.6 earthquake occurred in Hokkaido Eastern Iburi, Japan. Strong ground motion with a maximum 7 on Japan Meteorological Agency (JMA) seismic-intensity scale struck Atsuma in Eastern Iburi and south-east Hokkaido, causing 42 death, about 462 collapsed houses and about 1570 partially destroyed houses [1].

The hypocenter of this earthquake determined by the JMA is located beneath the western part of the Hidaka Collision Zone where an arc–arc collision system in Hokkaido Island is placed. The hypocenter depth is as deep as 37km in the Hidaka Collision Zone. The characteristics of strong ground motions from this earthquake occurring in deep crust are needed to compare with those from shallow crustal earthquake in other regions in Japan.

Stress parameter is one of the most important parameters for predicting strong ground motion. Miyakoshi [2] compiled the stress parameter of SMGAs of 13 inland crustal earthquakes estimated using the empirical Green's function method (EGMF). The average stress parameter of SMGA is 13.6 MPa almost the same as that of asperities determined by the waveform inversion analysis of strong motion data. Asano and Iwata [3] compiled the stress parameters of the asperities of inland crustal earthquakes by the waveform inversion analysis. They indicated that the stress parameters clearly depend on their depth. One of the deepest events analyzed by [3] is 18 km deep with stress parameter is approximately 23 MPa. There are not included deep events with the hypocenter depth of 37 km in their dataset.

Satoh [4] obtained a strong motion generation areas (SMGAs) model for the 2018 Hokkaido Eastern Iburi earthquake (called "the 2018 Iburi earthquake" hereafter) using the empirical Green's function method (EGFM), the maximum stress parameter for one of the SMGAs is 74.4 MPa in approximately 23 km depth. This result is extremely large, compared with shallow crustal earthquakes so far compiled by [2]. In this study, we construct the SMGA source model using the EGFM to confirm how large stress parameters are needed for reproducing strong ground motions from this earthquake. The accuracy of stress parameters of the SMGAs strongly depend the reliability of source parameters, in particular stress parameters, of the EGF events. The stress parameters are evaluated from seismic moment and corner frequency of observed motions from the EGF events. The corner frequencies are correctly determined using the source spectral ratio method independently from site and propagation-path effects. We reconfirm the corner frequencies estimating source spectra of the EGF events. Then the relation between seismic moment: M_0 and combined SMGAs area for this earthquake is compared with the conventional scaling relation. We also estimate stress parameters of aftershocks which occurred in the source area. Finally, we discuss the relationship between the stress parameter of SMGAs and depth.

2. Strong-Motion Data

The K-NET and KiK-net strong-motion observation networks operated by Japan's National Research Institute for Earth Science and Disaster Prevention (NIED) recorded strong ground motions at 473 stations during the 2018 Hokkaido Eastern Iburi earthquake.

The peak ground acceleration of 1796.4 gal and 1504.8 gal (absolute values calculated from the three components) were measured at K-NET stations HKD127 (Oiwake) and KiK-net stations IBUH01 (Oiwake), respectively, with almost the same hypocentral distance of 44.9km. Figure 1 (a) and (b) shows a map view of aftershock distribution and the locations of observed stations and observed records, respectively.

We used strong-motion data recorded at 3 surface K-NET and 5 underground KiK-net stations in the near-source regions to constrain the short-period source model. The observed records used as EGFs were band-pass-filtered from 0.5 to 10 Hz, taking the reliable frequency range for observed records of small events into account.

© The 17th World Conference on Earthquake Engineering

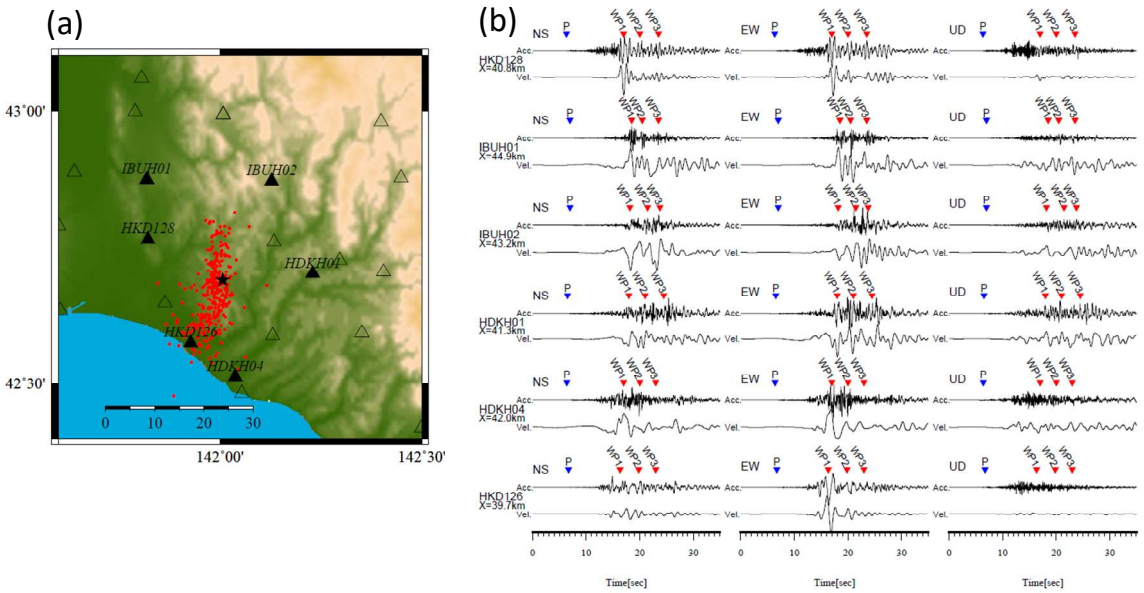

Figure 1 (a) Map view of strong-motion stations (black triangles) and aftershock distribution from the JMA unified hypocenter catalog (red dots). (b) Filtered observed acceleration (BPF: 0.1-10 Hz) and velocity (BPF: 0.1-1 Hz) records near the fault source area. Onset of P wave and distinctive wavepackets (WP1, WP2 and WP3) were indicated blue inverted triangle and red inverted triangle, respectively.

3. Locating Strong-Motion Generation Areas

We recognize three isolated wavepackets (WP1, WP2, and WP3) in the near-source region records as shown in Figure 1(b). We consider the locations of generating those wavepackets to correspond to the SMGAs.

First, we assumed a fault model of the mainshock consisting of three segments. Figure 2 shows aftershocks distribution from the JMA unified hypocenter catalog. The hypocenters of the JMA unified hypocenter catalog are similar to the calculated hypocenters using the DD method by NIED (2018).

We assume that the SMGAs are located on the source fault plane. In this study, we determined the locations of the SMGAs and those of the rupture starting point and rupture time for each SMGA objectively from the S-wave onset data and the travel time each station using [5]. The velocity structure models are approximated from the regional integrated velocity structure model by [6]. The difference between the observed and theoretical travel time at each station is corrected as uncertainty of velocity structure model using an Mw 4.3 aftershock as reference event. The optimal location and rupture time of the individual SMGA are determined minimizing the RMS calculated from the following equation by a grid search,

$$\mathrm{RMS} = \sqrt{\frac{1}{n}\sum_{i=1}^{n}\left[t_0 + \left(t^i_{\mathrm{cal}} - \hat{t}^i_{\mathrm{cal}}\right) - \left(t^i_{\mathrm{obs}} - \hat{t}^i_{\mathrm{obs}}\right)\right]^2}. \quad (1)$$

Here, t^i_{cal} and t^i_{obs} are the calculated and observed travel times of the SMGA at the *i*-th station, respectively. $\hat{t}^i_{cal}$ and $\hat{t}^i_{obs}$ are the calculated and observed travel times of the reference event, respectively. t_0 is the rupture time of an SMGA relative to the origin time of the mainshock. *n* is the number of stations used. The onset of the wavepackes at 6 to 13 staions are used for each SMGA. The observed record at IBUH01 and

© The 17th World Conference on Earthquake Engineering

HDKH01 are calculated to detect the three wavepackets generated from SMGA1, SMGA2 and SMGA3, as shown in Figure 3.

Figure 4 shows the estimated rupture starting points of three SMGAs projected on the map of plan view. SMGA1, SMGA2 and SMAG3 corresponding to WP1, WP2 and WP3 are located on southern segment and northern segment, respectively. The rupture delay times from the origin time are 5.5 s, 9.0 s and 13.0 s, respectively.

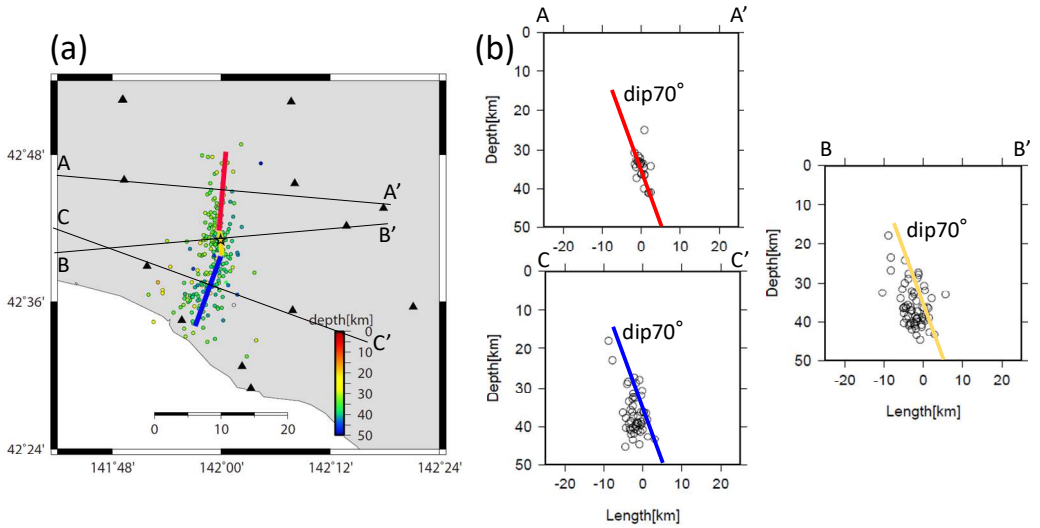

Figure 2 (a) Early aftershocks (color dots) within 6 hours from the mainshock and assumed fault plane model (red, yellow and blue lines). (b) Cross sections of aftershock distributions perpendicular to the fault plane.

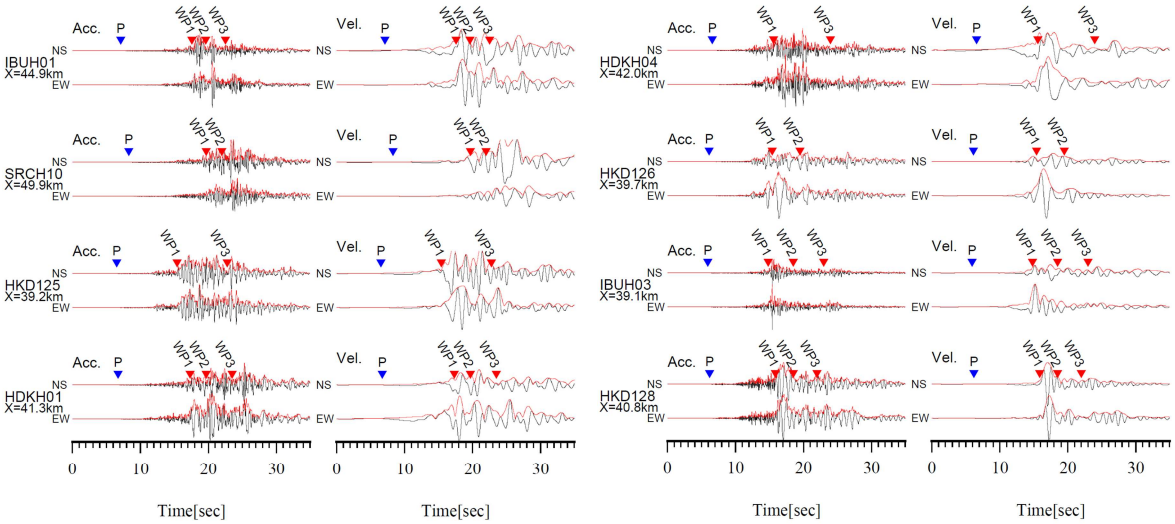

Figure 3 Onset of each wavepacket seen in acceleration and velocity waveforms. The blue and red triangles indicates P- and wavepachets onsets, respectively.

© The 17th World Conference on Earthquake Engineering

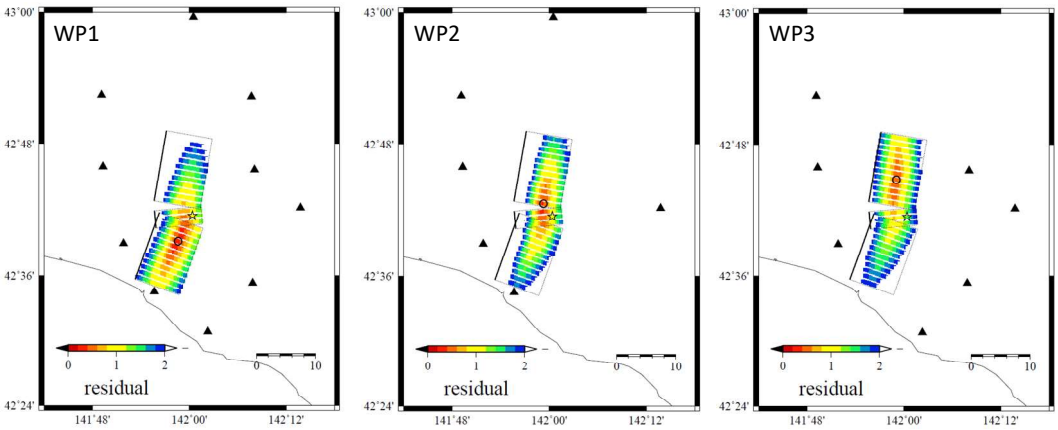

Figure 4 Distributions of RMS residuals estimated by the grid search method for locating the rupture starting points of SMGAs. The triangles indicate stations used for the grid search.

4. Ground motions simulation by the Empirical Green's Function (EGF) Method

4.1 Parameters of aftershocks as the empirical Green's functions

The sizes of aftershocks used as the EGFs (EGF events) should ideally be much smaller than the size of each SMGA. Moreover, the records of the EGF events must share common propagation paths, site effects, and radiation characteristics with the ground motions from SMGAs of interest. The conditions for the aftershock records usable as the empirical Green's functions are as follows: (1) the hypocenter of the EGF events should be near the asperities of the SMGA; (2) the radiation characteristics of the EGF events should be similar to the SMGA. The first condition is required to assure that the propagation-path effects of the EGF events are approximately the same as that of the SMGA. The second condition does not always mean that the source mechanism of the aftershock is the same as that of the SMGA. The second condition guarantee that the synthetic waveforms have almost the same directivity effects as the observed ones. On the other hand, the directivity effects are not so influential on high frequency motions more than 1 Hz although influential on lower frequency motions.

To calculate ground motions for each SMGA, we divide the area of the SMGA into N × M square subfaults, the area of which is set to be the same as the area of the EGF events. The ground motions from the SMGAs are expressed as a superposition of the EGFs.

According to temporal and spatial distribution of moment tensor on the mainshock fault plane by [7], the source mechanism is different in northern part and southern part of the fault plane they assumed. Therefore, we selected the records of two aftershocks (Mw4.3, EGF1 and Mw3.7, EGF2) as the empirical Green's function. The EGF1 event occurred near the SMGA1 and EGF2 did near the SMGA2 and the SMGA3. Therefore, the records of EGF1 are used as the empirical Green's functions for SMGA1 and the records of EGF2 as the empirical Green's functions for SMGA2 and SMGA3.

Next, we calculated the source areas and stress parameters of EGFs from the seismic moments and corner frequencies using [8, 9] formula. The corner frequencies were estimated by the source spectral ratio function method [10]. Figure 5 indicate the source spectral ratios of the mainshock to aftershock records used as the empirical Green's functions for EGF1 and EGF2. The source parameters of the EGF events are listed in Table 1

© The 17th World Conference on Earthquake Engineering

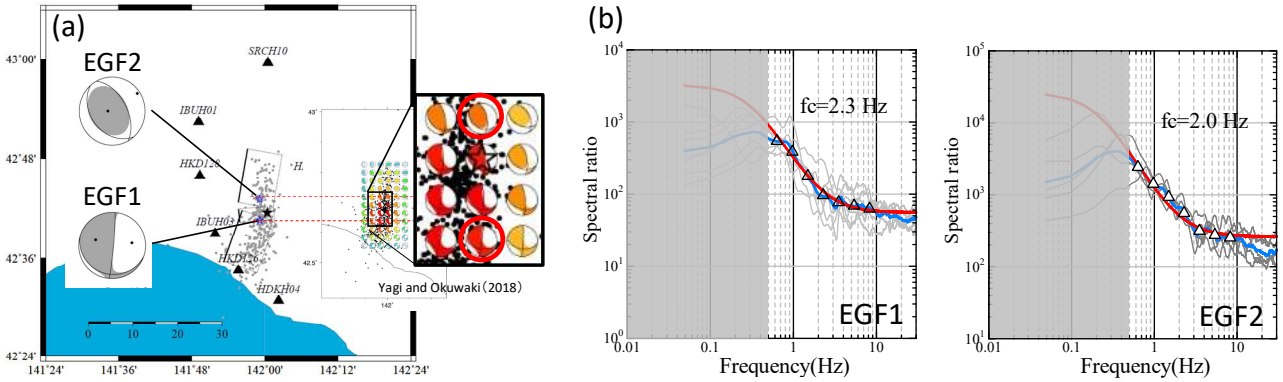

Figure 5 (a) Locations of EGF events and focal mechanisms of EGF events and moment tensor distributions [7]. (b) Source spectral rations of ground motions of the mainshock to those of the EGF events. The red and blue lines indicate the theoretical source spectral ratio and the observed source spectral ratio, respectively.

Table 1 Parameters of EGF events

	EGF 1	EGF 2
origin time※1	2018/9/24 18:17	2018/9/7 17:11
depth(km)※1	41.4	34.3
M_0 (Nm)※2	3.06E+15	3.82E+14
Mw※2	4.3	3.7
Vs (km/s)※3	4.0	4.0
corner frequency (Hz)	2.3	2.0
length of subfault(km)	1.1	1.3
stress parameter (MPa)	5	0.4

4.2 Estimation of SMGA source model

We have simulated the ground motions for the characterized source model using the EGF method [11] with a revised correction function [12]. We omit details of the EGF method here as they have been explained in previous research (e.g., [13, 14]).

The optimum source model is selected so as to minimize the residuals between the observed and synthetic ground motions, defined by the following equation [10, 15]:

Residual values

$$\text{Residual value} = \sum_{station} \sum_{component} \left\{ \frac{\sum_t (u_{obs} - u_{syn})^2}{\left[(\sum_t u_{obs}^2)(\sum_t u_{syn}^2) \right]^{1/2}} + \frac{\sum_t (a_{env,obs} - a_{env,syn})^2}{(\sum_t a_{env,obs})(\sum_t a_{anv,syn})} \right\} \quad (2)$$

where u_{obs} and u_{syn} are the observed and the synthesized displacement waveforms, and $a_{env,obs}$ and $a_{env,syn}$ are the observed and synthesized acceleration envelopes. The best-fit model is given from the minimum of the fitting function. Further, the residual is defined as the sum of the squared residuals of displacement waveforms and acceleration envelopes at KiK-net stations. On the other hands, at K-NET stations, the residual is defined as the sum of the squared residuals of displacement and velocity waveforms to avoid non-linear site effects on acceleration motions.

The parameters which characterize each SMGA are its area, rupture starting point in the SMGA, stress parameter ratio, risetime of EGF and rupture velocity.

© The 17th World Conference on Earthquake Engineering

The area of each SMGA and the rupture starting point inside the SMGA are shown in Figure 6. The source parameters of the best SMGA model is listed in Table 2. The average stress parameter for each SMGA should be assigned from empirical relations and has been found to be 27 - 35 MPa in this study.

Figure 7 displays comparisons between the observed and synthetic waveforms in the form of acceleration, velocity, and displacement. The synthetic waveforms at most of stations fit the observations reasonably well. Figure 8 shows comparisons between the observed and synthetic pseudo velocity response spectra. Figure 9 shows comparisons between the observed and synthetic waveforms from each SMGA. The waveform of southern stations from rupture start point (HKD126) are strongly influenced by SMGA1. Especially, these stations are affected by directivity due to forward rupture propagation on SMGA1. The waveform of northern stations from rupture start point (IBUH01, HDKH01) are largely influenced by SMGA2. Three packet wave (WP1, WP2 and WP3) on observed record are contributed by SMGA1, SMGA2 and SMGA3, respectively.

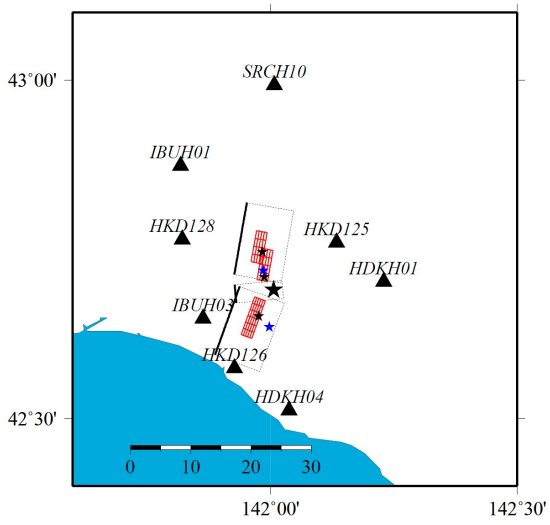

Table 2 Parameters of the best SMGA source model

	NL	NW	NT	C	NSL	NSW	risetime of EGFs
SMGA1	6	5	5	7	4	5	0.08sec
SMGA2	4	4	4	69.3	1	3	0.15sec
SMGA3	4	4	4	69.9	2	3	0.16sec

	Vr	L	W	stress parameter	seicmic moment	rise time	rag time
SMGA1	2.9km/s	6.6km	5.5km	35.0MPa	3.21×10^{18}Nm	0.4sec	5.5sec
SMGA2	2.9km/s	5.2km	5.2km	27.7MPa	1.69×10^{18}Nm	0.6sec	9sec
SMGA3	2.9km/s	5.2km	5.2km	28.0MPa	1.71×10^{18}Nm	0.64sec	13sec

Figure 6 Layout of three segments (black rectangles) and SMGAs (SMGA1, SMGA2, and SMGA3 red rectangles) in the respective three segments.

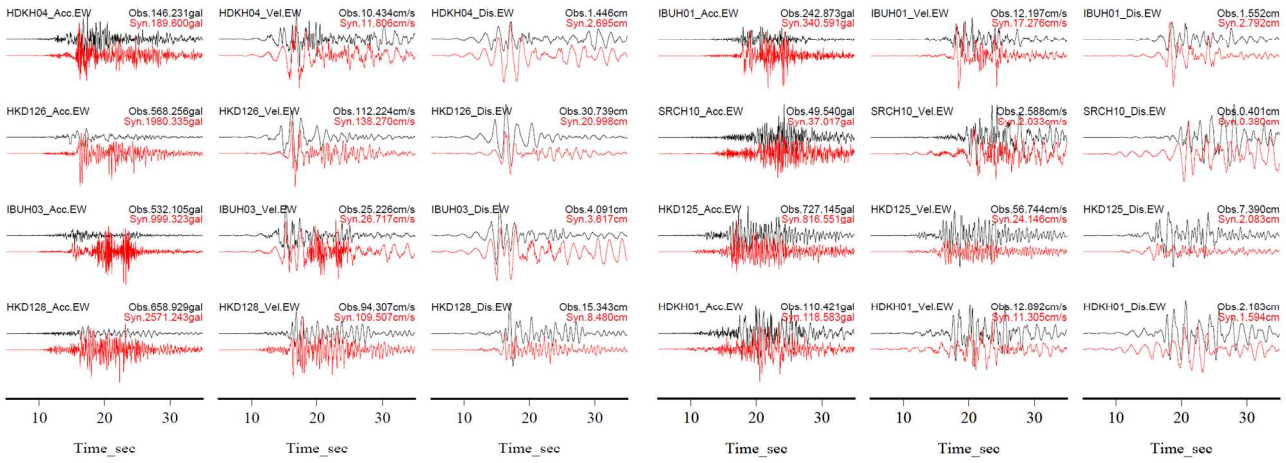

Figure 7 Comparison between observed (black) and synthetic (red) waveforms (acceleration, velocity, and displacement) in the EW components of the mainshock. The numerical in the upper of each waveform express the maximum amplitude.

© The 17th World Conference on Earthquake Engineering

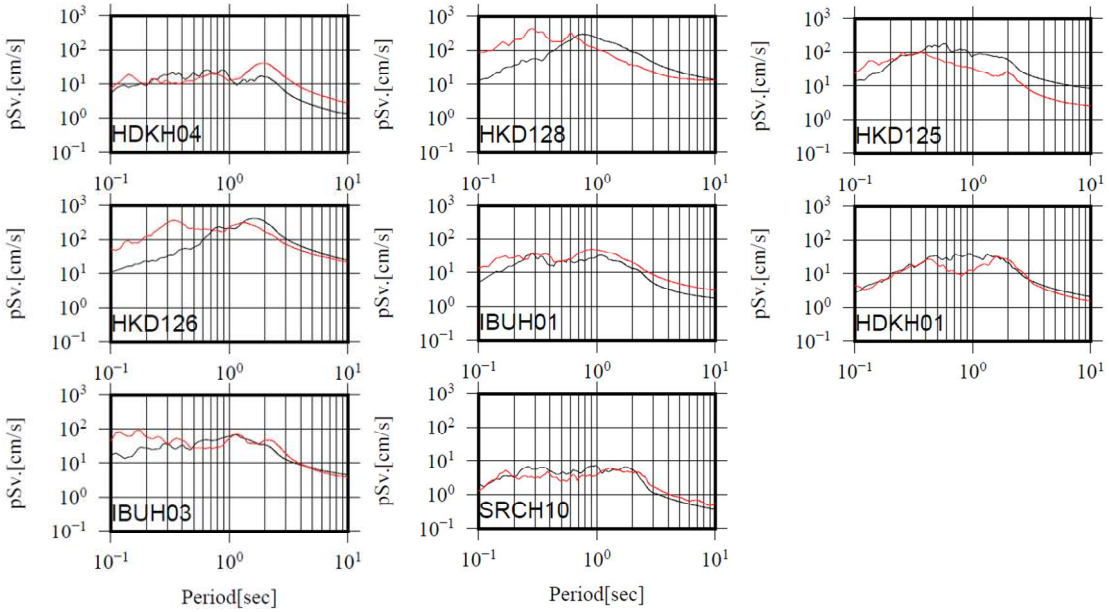

Figure 8 Comparison of pseudo-velocity spectra (damping ratio h=0.5 %) between observed (black) and synthetic (red) ground motions of the mainshock.

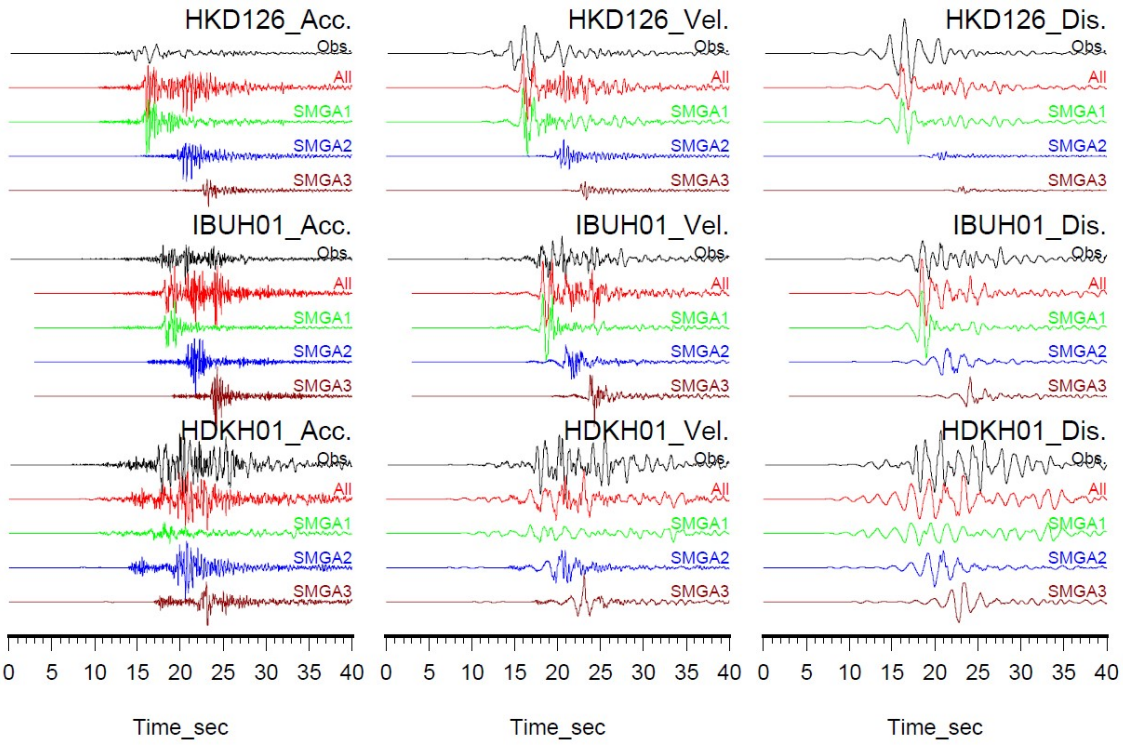

Figure 9 Comparison of observed and synthetic waveforms (acceleration, velocity and displacement) from each SMGA at three stations (HKD126, IBRH01, and HDKH01). From upper of each station, observed (black), synthetic (red), contributions from SMGA1 (green), SMGA2 (blue), and SMGA3 (brown) are drawn.

© The 17th World Conference on Earthquake Engineering

5. Discussion

First, the best-fit SMGA model we estimate is compared with the slip distributions obtained from waveform inversion of strong motion data by [16] and [17] in Figure 10. Large slips obtained by those two groups are seen commonly in southern area from the mainshock hypocenter in the center and right of Figure 10. These large slips are considered to be SMGA1. Large slips corresponding to SMGA2 and SMGA3 can be seen in the slip distributions in the center of Figure 10.

Next, we discuss the relationship between the seismic moment and the combined area of SMGAs. The relationship of the seismic moment versus the combined SMGAs area for this earthquake is plotted with the corresponding scaling relationship by [18] in Figure 11 (red circle). The combined areas of SMGAs deviates smaller from the relationship between seismic moment and the combined area of asperities by [19].

Finally, we discuss the stress parameters of the mainshock and aftershocks which occurred within the source area. We target aftershocks with Mw 4.0- 4.9. The stress parameter of the aftershocks were estimated from their corner frequencies using [8, 9]. S-wave velocity: Vs of bedrock in source area is used 4.0km/s. The procedure of estimating the corner frequencies are the same as that of the EGF event (hereinafter called Method 1). In addition, we estimated the corner frequency directly from the relationships between theoretical source spectra and the displacement observed source spectra of aftershocks (hereinafter called Method 2). The observed source spectra were estimated to remove propagation-path and site effects from the observed spectra at each station. The site effects at each station was estimated from Japan Integrated Velocity Structure Model: JIVSM [6] by the S wave multiple reflection theory. We confirmed that the corner frequencies estimated by Method 1 and the corner frequencies evaluated by Method 2 are approximately the same in our previous studies. Figure 12 shows comparison between corner frequencies from the source spectral ratios and those from the source displacement spectra. This result suggests that the corner frequencies estimated from the source ratio function method are robust [10]. Figure 13 (a) indicates the depth dependency on the stress parameter (red circle) of aftershocks of the 2018 Iburi earthquake from their corner frequencies using the source spectral ratio method. Stress parameters of shallow crustal earthquakes by [20] versus depth are also plotted. The stress parameters of the aftershocks seem to be larger than those of the shallow inland crustal earthquake. Figure 13 (b) shows the stress parameters of the SMGAs in this study versus the depth with the regression line by [18]. The stress parameter of the mainshock (27-35MPa) are an extension of the regression line by [18].

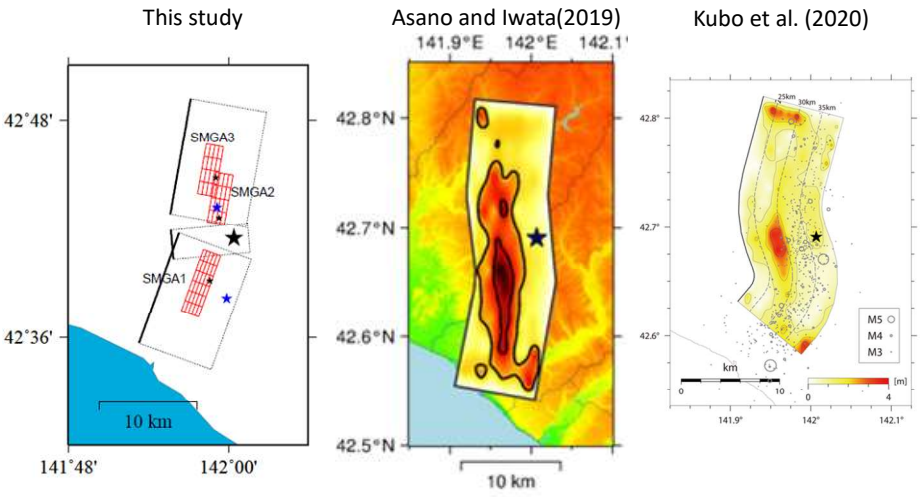

Figure 10 Comparison between the SMGAs (SMGA1, SMGA2 and SMGA3) in this study (left) and the slip distributions from the inversions [16] and [17] (center and right).

© The 17th World Conference on Earthquake Engineering

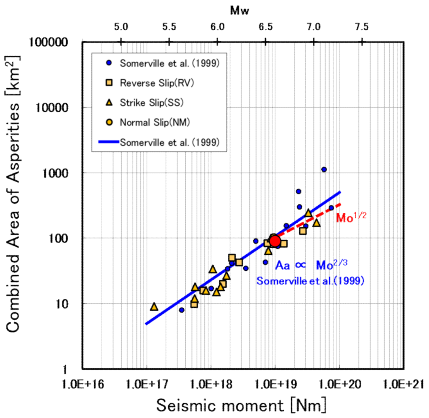

Figure 11 Relationship between combined area of asperities and seismic moment by [18, 19]. The sum of three SMGAs is regarded to be equivalent to combined area of asperities. Combined area of SMGAs of this earthquake is drawn by red circle.

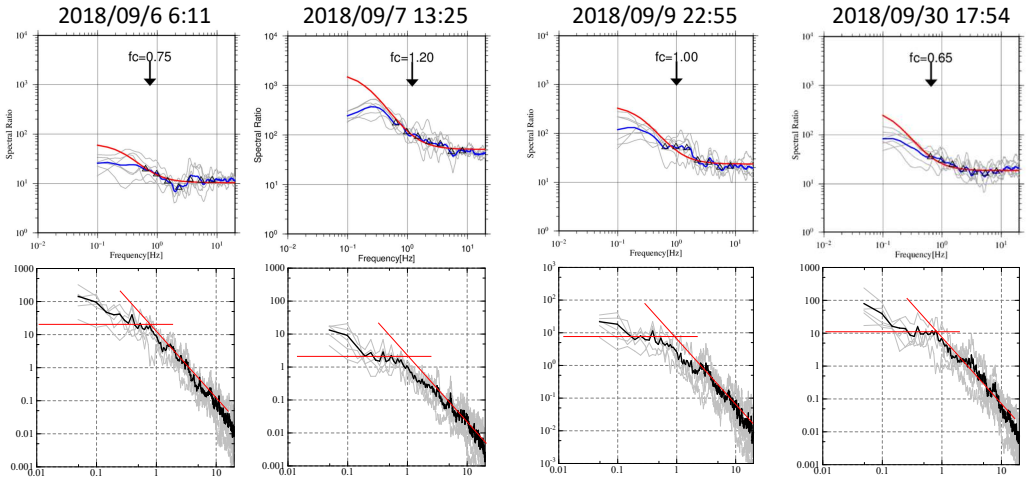

Figure 12 Comparison between corner frequencies from the source spectral ratios (upper) and those from the source displacement spectra (lower).

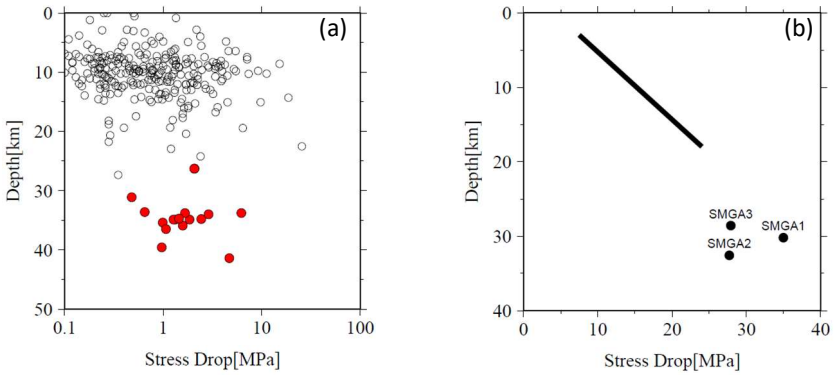

Figure 13 (a) Average stress parameter versus depth. The red circles indicate stress parameters of aftershocks of this earthquake. The open circles indicate stress parameters of inland crustal earthquake in Japan by [20]. (b) Stress parameter of SMGA versus depth. The regression line (black) is from [3].

© The 17th World Conference on Earthquake Engineering

6. Conclusion

We estimated strong motion generation area (SMGA) source model for the 2018 Hokkaido Iburi earthquake using forward modeling by comparing the observed records with synthetic motions based on the characterized source model [10,15] and the EGF method [12]. The observed strong motion records of the mainshock exhibit three distinct wavepackets that correspond to specific three SMGAs, respectively.

We successfully simulated ground motions from the three SMGAs using observed records of two aftershocks occurring near the SMGAs as EGFs. SMGA1 is located in the southern part segment from the hypocenter of the mainshock; SMGA2 and SMGA3 are located in the northern part segment from the hypocenter. The locations of the SMGAs are almost consistent with large slip areas by the waveform inversion analysis of strong motion data. The combined area of the SMGAs is smaller than predicted values from the scaling relationship [18, 19]. The stress parameters of the SMGAs are 27-35MPa, which are higher than those of shallow inland crust earthquakes.

Finally, we find that the stress parameters of aftershocks of this earthquake tend to be higher than those of shallow inland crustal earthquakes by [20]. The stress parameter of each SMGA of the mainshock evaluated at 27-35 MPa is larger than those of the aftershocks. The stress parameters of the SMGAs of the mainshock and aftershocks of this earthquake have possibly dependence on scale as well as source depth.

7. Acknowledgements

We use the waveforms published by K-NET, KiK-net. We illustrated the few graphs using GMT (Wessel and Smith 1998).

8. Copyrights

17WCEE-IAEE 2020 reserves the copyright for the published proceedings. Authors will have the right to use content of the published paper in part or in full for their own work. Authors who use previously published data and illustrations must acknowledge the source in the figure captions.

9. References

[1] Fire and Disaster Management Agency (2018): On January 28, 2019 Hokkaido eastern Iburi earthquake, http://www.bousai.go.jp/updates/h30jishin_hokkaido/pdf/310128_jishin_hokkaido.pdf. (in Japanese).

[2] Miyakoshi K, Irikura K and Kamae K (2015): Re-examination of scaling relationships of source parameters of the inland crustal earthquakes in Japan based on the waveform inversion of strong motion data, *Journal of Japan Association for Earthquake Engineering, Vol. 15 Issue 7, 141 -156.*

[3] Asano K and Iwata T (2011): Characterization of Stress Drops on Asperities Estimated from the Heterogeneous Kinematic Slip Model for Strong Motion Prediction for Inland Crustal Earthquakes in Japan, *Pure Appl. Geophys. 168, 105-116.*

[4] Satho T (2019): Broadband source model and strong motions of the 2018 Hokkaido eastern Iburi earthuake. *The Architectural Institute of Japan's Journal of Structural and Construction Engineering (763), 1175-1185.*

[5] Asano K and Iwata T (2012): *Source model for strong ground motion generation in the frequency range 0.1-10 Hz during the 2011 Tohoku earthquake, Earth Planets Space, 64, 1111-1123.*

[6] Koketsu K, Miyake H and Suzuki H (2012): *Japan integrated velocity structure model version 1. Proceedings of the 15th world conference on earthquake engineering, Lisbon, Portugal, September, 24-28, 2012.*

[7] Yagi Y and Okunuki R (2018): 2018 Hokkaido eastern Iburi earthquake, http://www.geol.tsukuba.ac.jp/~yagi-y/EQ/20180905/index.html.

[8] Brune, J. N. (1970). Tectonic stress and the spectra of seismic shear waves from earthquakes, *J. Geophys. Res. 75, 4997–5009.*

© The 17th World Conference on Earthquake Engineering

[9] Brune, J. N. (1971). Correction, *J. Geophys. Res. 76, 5002.*

[10] Miyake H, Iwata T and Irikura K (1999). Strong ground motion simulation and source modeling of the Kagoshima-ken Hokuseibu earthquake of March 26 (MJMA 6.5) and May 13 (MJMA 6.3), 1997, using empirical Green's function method, *Zisin 51, 431–442 (in Japanese with English abstract).*

[11] Irikura, K. (1986). Prediction of strong acceleration motions using empirical Green's function, in Proc. *7th Japan Earthq. Eng. Symp., Tokyo, 10–12 December, 151–156.*

[12] Irikura K., Kagawa T and Sekiguchi H (1997). Revision of the empirical Green's function method by Irikura (1986), *Program and abstracts, Seismol. Soc. Japan 2, B25 (in Japanese).*

[13] Kamae K and Irikura K (1998). Rupture process of the 1995 Hyogo-ken Nanbu earthquake and simulation of near-source ground motion, *Bull. Seismol. Soc. Am. 88, 400–412.*

[14] Kurahashi S and Irikura K (2010). Characterized source model for simulating strong ground motions during the 2008 Wenchuan earthquake, *Bull. Seismol. Soc. Am. 100, 2450–2475.*

[15] Miyake H, Iwata T and Irikura K (2003), Source characterization for broadband ground-motion simulation, Kinematic heterogeneous source model and strong motion generation area, *Bull. Seism. Soc. Am., 93, 2531–2545.*

[16] Asano K and Iwata T (2019): Source rupture process of the 2018 Hokkaido Eastern Iburi earthquake deduced from strong-motion data considering seismic wave propagation in three-dimensional velocity structure. *Earth, Planets and Space, 71.*

[17] Kubo H, Iwaki A, Suzuki W, Aoi S and Sekiguchi H (2020): Estimation of the source process and forward simulation of long-period ground motion of the 2018 Hokkaido Eastern Iburi, Japan, earhtuqkae. *Earth, Planets and Space, 72.*

[18] Miyakoshi K, Somei K, Yoshida K, Kurahashi S, Irikura K and Kamae K (2019): Scaling Relationships of Source Parameters of Inland Crustal Earthquakes in Tectonically Active Regions, *Pure Appl. Geohys., 121* .

[19] Somerville P, Irikura K, Graves R, Sawada S, Wald D, Abrahamson N, Iwasaki Y, Kagawa T, Smith N, and Kowada A: Characterizing crustal earthquake slip models for the prediction of strong ground motion. *Seism. Res. Lett., 70, 1999, pp.59-80*

[20] Somei K, Asano K, Iwata T and Miyakoshi K (2014): Source Scaling of Inland Crustal Earthquake Sequences in Japan Using the S-Wave Coda Spectral Ratio Method, *Pure Appl. Geophys., 171, 2747-4766.*

[21] Wessel P, Smith WHF (1998): New, improved version of the generic mapping tools released. *EOS Trans AGU 79:579.*

© The 17th World Conference on Earthquake Engineering